

Structure and dynamics of a pinned vortex liquid in a superconducting a -Re₆Zr thin film

Rishabh Duhan,^{1,*} Subhamita Sengupta,^{1,†} Ruchi Tomar^{1,‡}, Somak Basistha,¹ Vivas Bagwe¹,
Chandan Dasgupta² and Pratap Raychaudhuri^{1,‡}

¹Tata Institute of Fundamental Research, Homi Bhabha Road, Colaba, Mumbai 400005, India

²Department of Physics, Indian Institute of Science, Bangalore 560012, India

 (Received 26 April 2023; revised 3 August 2023; accepted 17 October 2023; published 8 November 2023)

We report the formation of a pinned vortex liquid spanning a very large region of the magnetic field-temperature parameter space in a 5-nm-thick amorphous superconducting Re_xZr ($x \approx 6$) (a -ReZr) thin film, using a combination of low-temperature scanning tunneling spectroscopic (STS) imaging and magnetotransport measurements. The nature of the vortex liquid differs significantly from a regular liquid. Analyzing series of STS images captured as a function of time, we observe that the interplay of pinning and intervortex interactions produces a very inhomogeneous state, where some vortices remain static, whereas others move forming a percolating network along which vortices are mobile. With increase in temperature or magnetic field this network becomes denser, eventually encompassing all vortices. Our results provide key insight on the nature of a pinned vortex liquid and some of the peculiarities in the transport properties of ultrathin superconducting films.

DOI: [10.1103/PhysRevB.108.L180503](https://doi.org/10.1103/PhysRevB.108.L180503)

In recent years there has been renewed interest in the mixed state in thin superconducting films, owing to the observation of vortex fluid states [1–4] in these materials. On general grounds, it is expected that in a clean superconductor the crystalline vortex lattice can melt at a characteristic temperature/magnetic field, producing a vortex liquid (VL) state. So far, VL states in bulk single crystals have been unambiguously detected only in layered high- T_c cuprates [5–8] at large operating temperatures. On the other hand, for conventional superconductors, the vortex lattice is either seen to retain its crystalline structure till very close to the upper critical field (H_{c2}) line [9,10] (in extremely clean crystals) or is driven into a disordered vortex glass above the order to disorder transition [11–13]. The situation is different in thin films, where reduced dimensionality renders the vortex lattice more susceptible to thermal (and quantum [14,15]) fluctuations. Indeed, in weakly pinned superconducting thin films, two-dimensional (2D) VL states with different long-range and short-range correlations, such as isotropic, hexatic, and smectic, have been identified using real space imaging of the vortex state [2–4].

When a current is passed in the mixed state of a superconductor, each vortex experiences a Lorentz force, $F_L = J\Phi_0 t$ (where J is the current density, $\Phi_0 = h/2e \approx 2.068 \times 10^{-15}$ Wb is the flux quantum, and t is the thickness of the sample), which can cause the vortices to move and give rise to dissipation. When vortices form a crystalline solid, a finite density of weak pinning centers can collectively pin all the vortices, such that the dissipation happens only above a critical current [16,17] I_c , where the F_L overcomes the pinning force. In a VL a finite density of pins cannot pin all vortices, except for the extreme situation where each vortex is individ-

ually pinned. However, it has been theoretically predicted that in two dimensions, such a vortex glass is unstable [18–20] except at $T = 0$. On the other hand, various inhomogeneous liquid states [21,22] such as interstitial liquid or vortex slush [23–25] have been proposed, where the motion of vortices is dictated by a combination of defect pinning and interaction with nearby vortices. Understanding the structure and dynamics of the pinned VL is not only important to realize the application potential of these materials, but also connects to the fundamental problem of a pinned liquid that is relevant for a variety of systems; e.g., colloids [26], skyrmion lattices [27], liquid-crystal molecules, or lipids in membranes [28].

Scanning tunneling spectroscopy (STS) imaging is a powerful tool to obtain structural information of the vortex lattice [29]. Here, a fine conducting tip of a low temperature scanning tunneling microscope [30] (STM) is brought within the tunneling range of a superconductor, and the local density of states (LDOS) is measured from a spatially resolved tunneling conductance map, $G(V, \mathbf{r}) = \frac{dI(\mathbf{r})}{dV}|_V$ (\mathbf{r} is the local coordinate on the surface), while rastering the tip over the sample surface. Since both the superconducting energy gap and the coherence peak in the LDOS is suppressed at the normal core of a vortex, each vortex manifests as a local minimum [13] in $G(V, \mathbf{r})$ when the bias voltage is kept close to the coherence peak. This technique has been extensively used to image crystalline and glassy vortex states. However, application of STS in a VL is trickier. Since STS imaging is a slow measurement, imaging of moving vortices has mostly been restricted to situations where the motion is very slow [1,3,4,31–33]. When the movement of vortices is faster than the characteristic time of data acquisition at every pixel (few milliseconds), rapid fluctuation due to moving vortices will get integrated out, thus blurring the boundary between the vortex core and the gapped superconducting region outside [14]. The measured $G(V, \mathbf{r})$ at any point will thus be an average of the contribution both from inside and outside the vortex core, and its value

*rishabh.duhan@tifr.res.in

†subhamita.sengupta@tifr.res.in

‡pratap@tifr.res.in

will depend on how frequently a vortex came below the tip. Consequently, $G(V, \mathbf{r})$ can be considered as a metric of the probability density of vortices, where its lowest value would correspond to a static vortex located at point \mathbf{r} , and the highest value would be for a location \mathbf{r} that is far from any vortex. For a homogeneous vortex liquid where the probability of finding a vortex is the same everywhere, $G(V, \mathbf{r})$ would be spatially uniform, and its value will be in between these two extremes. On the other hand, if there is a set of preferred points \mathbf{r}_i , where vortices spend longer time (as expected for a pinned liquid), $G(V, \mathbf{r})$ would display local minima at \mathbf{r}_i but the value at the minima, $G^{\text{min}}(\mathbf{r}_i)$, will depend on the fraction of time a vortex spends there. In this interpretation, $G(V, \mathbf{r})$ provides a measure [34] of the time-averaged LDOS of vortices at point \mathbf{r} . In this Letter, we use this information from STS images to investigate the structure and dynamics of a pinned vortex liquid in a thin superconducting film.

Our sample consists of a 5-nm-thick amorphous Re_xZr , $x \approx 6$ ($a - \text{ReZr}$) superconducting film ($T_c \sim 4.65$ K) grown on oxidized Si substrate using pulsed laser deposition [35]. The coherence length and penetration depth [36] are $\xi \sim 5.9$ nm and [35] $\lambda(T \rightarrow 0) \sim 800$ nm respectively. The STM topographic image shows a very smooth surface with very low density of particulates [36]. Here, pinning is not deliberately introduced, but rather arises naturally from substrate imperfections as the film thickness is reduced [36]. For this thickness the vortex lattice always remains in a disordered state with no evidence of hexatic or smectic order. For STS measurements the sample was transferred directly from the deposition chamber into the STM using an ultrahigh vacuum suitcase without exposure to air. For transport measurements, the same sample was subsequently covered with a 1.5-nm-thick Ge capping layer to prevent oxidation, and then patterned into a Hall bar using argon ion beam milling. Resistance (R) as a function of temperature (T) and magnetic field (H) was measured in conventional four-probe geometry in a ^3He cryostat.

Figure 1(a) shows R - T in various magnetic fields (H) measured using a very small applied current, $I = 500$ nA, which is more than two orders of magnitude smaller than I_c obtained by linearly extrapolating back the slope of the flux flow region [37] of the current-voltage (I - V) characteristics at low temperatures [Fig. 1(c)]. The transport is thus in the thermally activated flux flow (TAFF) regime, where the vortex motion happens through thermally activated jumps over pinning barriers U . In a VL for $I \ll I_c$, TAFF is predicted to give a temperature dependent linear electrical resistance [21]. In our sample, at 410 mK we can resolve this linear region above 40 kOe [Fig. 1(d)]. We observe that the R - T curves follow a simple activated behavior, $R = R_0 e^{-U(H)/kT}$ (k is the Boltzmann constant), from a few Kelvin below T_c down to the temperature where the data hit the noise floor [Fig. 1(b)]. This activated behavior is a hallmark of the putative pinned VL [21] where U is independent of current. In contrast, in a vortex glass [17,4] the pinning barrier diverges at small current as $U(I) \propto (\frac{I_0}{I})^\alpha$, where $I_0 \sim I_c$ and α is a constant or the order of unity. Consequently, in a vortex glass state the TAFF resistance becomes extremely small for $I \ll I_c$. Therefore, a transition to a vortex glass is marked by an abrupt decrease in the resistance at a characteristic temperature which we do not

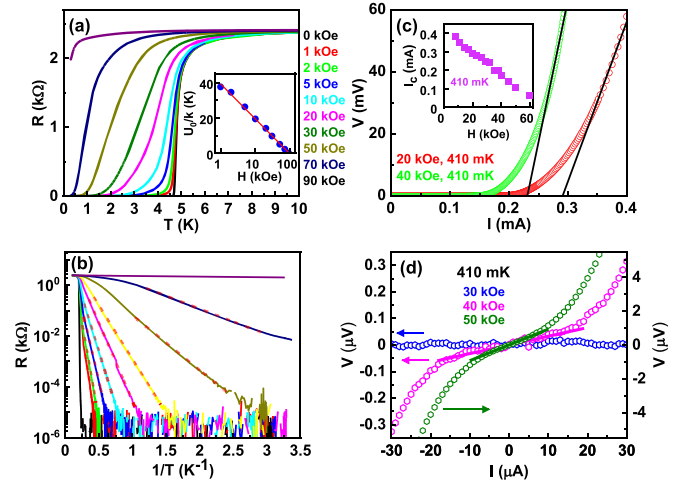


FIG. 1. (a) R vs T and (b) R vs $1/T$ (in semilog scale) in different magnetic fields (H); the red dashed lines in (b) are fits to the activated behavior, $R = R_0 e^{-U(H)/kT}$. Inset of (a) shows H dependence of activation energy $U(H)/k$ in semilog scale; the solid line is a fit to $U(H) = U_0 \ln(H_0/H)$, where $U_0/k \approx 8.6$ K and $H_0 = 94$ kOe. (c) Representative current-voltage (I - V) characteristics at $T = 410$ mK for different magnetic fields. I_c is determined from the I intercept of the extrapolated linear fits (black line) to the flux flow regime. Inset: H dependence of I_c at $T = 410$ mK. (d) Expanded view of representative I - V curves at $T = 410$ mK for different magnetic fields. Solid lines show the linear fit to the TAFF region.

observe in our sample. The magnetic field dependence of U [inset of Fig. 1(a)] fits well to a function of the form $U(H) = U_0 \ln(H_0/H)$, with $U_0/k \approx 8.6$ K and $H_0 \approx 94$ kOe $\sim H_{c2}$ (also see Supplemental Material Fig. 1S [36]). This functional form is observed in many superconducting films [38–41] and is expected when transport is dominated by the thermal activation of dislocation pairs. From theory [42,38], $U_0 = \frac{\Phi_0^2 I}{256\pi^3 \lambda^2}$ in CGS units; using [35] $\lambda = 800$ nm we obtain $U_0/k \sim 3.1$ K which is of the same order as that obtained from the fit. An agreement even at this level is remarkable considering the complexity of the vortex motion that we will highlight below.

We now concentrate on the STS data. We first focus on the data taken at 410 mK, 10 kOe. Except otherwise stated, the vortex state was always created by applying the magnetic field after cooling the sample to the base temperature in zero field, i.e., the zero-field-cooled (ZFC) protocol. We acquired ten successive $G(V, \mathbf{r})$ maps over an area containing approximately 120 vortices, where each map takes approximately 12 min to acquire. In Fig. 2(a) we show the normalized conductance maps, $G_N(V, \mathbf{r})$, for the first image. The conductance scale is normalized and stretched such that the lowest and highest values of $G_N(V, \mathbf{r})$ across all ten images correspond to -1 and 0 respectively. First, we concentrate on the individual image. $G_N(V, \mathbf{r})$ maps show the presence of local minima [$G_N^{\text{min}}(V)$] where the vortices are preferentially located, forming a disordered lattice with short range hexagonal coordination. However, the values of $G_N(V, \mathbf{r})$ at the minima as well as in between two adjacent minima have wide variations. Only some of these local minima are deep, i.e., $G_N^{\text{min}}(V) < -0.8$, and are separated from adjacent minima

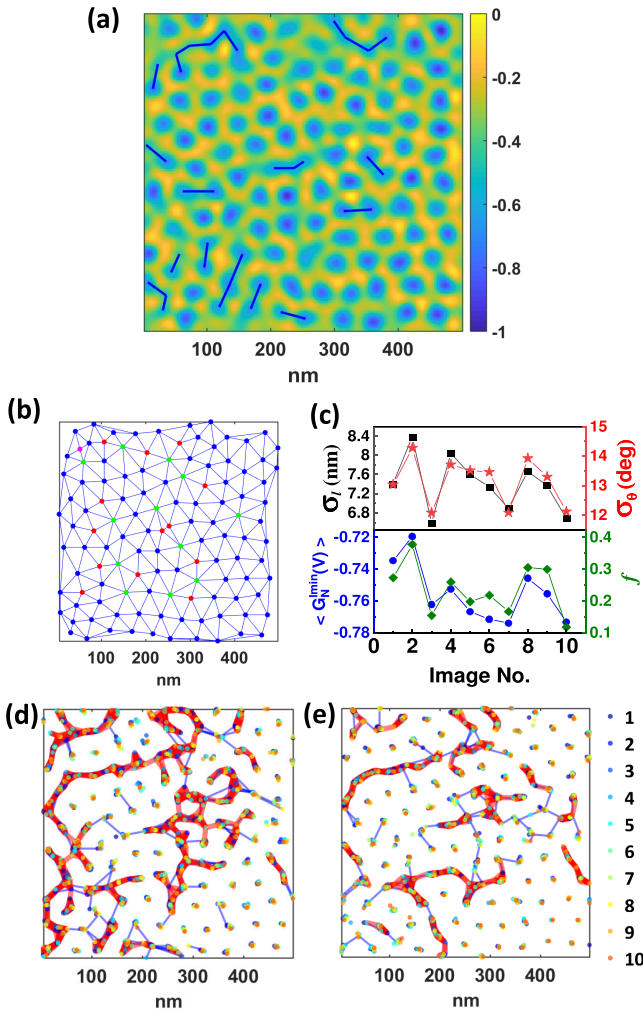


FIG. 2. (a) Representative $G_N(V, r)$ map of the first image of ten consecutive vortex images taken at 410 mK, 10 kOe. Blue lines show the motion paths of vortices. (b) Delaunay triangulation of local $G_N(V, r)$ minima (solid dots) for the image shown in (a); topological defects are color coded as magenta, red, and green corresponding to four-, five-, and sevenfold coordination, respectively. (c) Variation of σ_l (square), σ_θ (star), $\langle G_N^{\text{min}}(V) \rangle$ (circle), and f (diamond) for ten consecutive vortex images. (d) Positions of $G_N(V, r)$ minima obtained from all ten images, where minima corresponding to each image is shown in a different color; the red and blue networks represent the global motion paths of vortices. (e) Same as (d) but for the vortex state prepared using field cooled protocol.

with barriers where $G_N(V, r)$ is high. These minima appear at around the same location in every image. Here the vortices are localized and undergo only small displacement around their mean positions. On the other hand, we see several shallower minima corresponding to sites where the vortices are partially localized. All these sites contain at least one neighboring shallow minimum to which the vortex can hop; since this necessarily means that there is also a finite probability to find the vortex anywhere between these two minima, the maximum along the line joining them is also suppressed. To elucidate this more clearly, we connect all adjacent minima for which $G_N^{\text{min}}(V) > -0.8$ and where along the line joining the two

minima, $G_N(V) < -0.4$ using thin blue lines. The connected points define the motion paths along which the vortices hop from site to site within the time scale of acquisition of a single image. In order to understand the correlation between the structure of the lattice formed by the conductance minima and dynamics of vortices, in each image first we Delaunay triangulate the positions of the minima [Fig. 2(b)] to uniquely define the nearest neighbors for each point, and calculate four metrics. The degree of localization of vortices which is quantified by the average value of all the conductance minima, $\langle G_N^{\text{min}}(V) \rangle$, and the fraction of minima that are connected to the motion paths (f); and the structural distortion which is quantified by the two metrics: (i) $\sigma_l = (\frac{1}{N_l} \sum_i (l_i - a_H)^2)^{1/2}$, where l_i is the length of the i th bond, $a_H = 1.075(\frac{\Phi_0}{B})^{1/2}$ (where B is magnetic field in Tesla) is the expected lattice constant for a hexagonal vortex lattice (48.88 nm at 10 kOe) and N_l is the total number of bonds, and (ii) $\sigma_\theta = (\frac{1}{N_\theta} \sum_j (\theta_j - 60^\circ)^2)^{1/2}$, where θ_j s are the angles formed by two adjacent bonds starting from the same point, and N_θ is the total number of such angles. For a perfect hexagonal lattice, $\sigma_l = \sigma_\theta = 0$. In Fig. 2(c) we plot $\langle G_N^{\text{min}}(V) \rangle$, f , σ_l , and σ_θ for each image. We observe a clearly discernible correlation: When σ_l and σ_θ are low, $\langle G_N^{\text{min}}(V) \rangle$ and f are also low implying that when the lattice is less distorted the vortices on the average are more localized and vice versa. Therefore, we conjecture that the vortex motion is associated with a successive buildup of local strain and strain relaxation that happens over a time scale of minutes, even though the actual motion of vortices could be much faster.

To investigate the motion over longer time scales, in Fig. 2(d) we plot all the motion paths obtained from all ten images in a single frame (blue lines), which form an interconnected network. In the same figure we also show the positions of minima obtained from ten successive images using filled circular dots of different color for each image. We observe that the positions of some of the shallow minima change from one image to another (also see Fig. 12S [36]). The reason for this is that some vortices do not undergo a “complete” hop from one minimum to another, but instead get trapped in a pinning center midway, so that the corresponding $G_N(V, r)$ minima appear at a different location in the next image. To capture the network arising from motions that involve an incomplete hop we also connect any two points on this image that are separated by a distance $d < 0.5a_H$ (thick red lines) [36], eliminating any isolated segment that is shorter than $0.5a_H$ in length, since those correspond to the meandering motion of a vortex about its mean position. The two networks together capture the global motion paths of vortices. It is noteworthy that minima from two successive images do not necessarily appear as adjacent points on this global motion path, implying that the temporal evolution of the minima is faster than the time interval between imaging the same location in two successive images. To find out how robust this network is we repeated the measurement over the same area by heating the sample above T_c and cooling it back in the field-cooled (FC) protocol [Fig. 2(e)]. Despite the large thermal cycling and difference in the H - T cooling protocol, we observe that global motion paths are similar, showing that the motion paths of vortices are primarily dictated by underlying defect pinning.

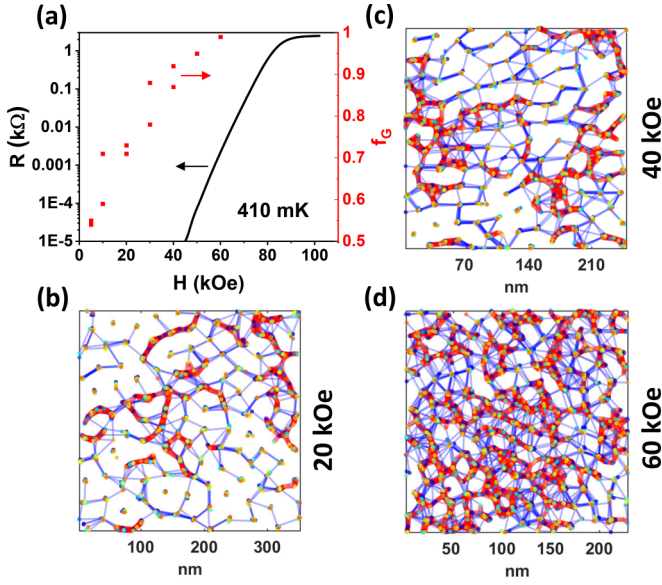


FIG. 3. (a) Variation of R and f_G with H at 410 mK. At some fields f_G were calculated from two sets of images taken at two different areas to get an estimate of statistical error. (b)–(d) Positions of $G_N(V, \mathbf{r})$ minima at three representative magnetic fields obtained from ten consecutive images along with global motion paths of vortices; the color scheme is the same as Fig. 2(d).

We now investigate the vortex states at different magnetic fields created using ZFC protocol at 410 mK. Figure 3(a) shows R - H measured at 410 mK. In Figs. 3(b)–3(d) we show the gradual evolution of the network of global motion paths with increasing field constructed from ten images in the same way. With increase in field, the network become denser, eventually, connecting almost all local minima across the ten images. To quantify this, we plot in Fig. 3(a) the fraction of all minima in all ten images, f_G , that are connected to at least one motion path. f_G increases smoothly with magnetic field. It is interesting to note that even though R falls below our resolution limit of 5 mΩ below 40 kOe, down to 1 kOe we do not observe [36] a situation where the local minima in $G_N(V, \mathbf{r})$ appear at the same location in all ten images, as would have been expected for a vortex glass. However, within the size of our images we cannot rule out the existence of a percolative transition that would mark the onset of long-range diffusion of vortices [43].

The temperature evolution of global motion paths at 10 kOe are shown in Figs. 4(a)–4(c) (see additional data in Fig. 4S [36]). All images are acquired on the same area by correcting any thermal drift using topographic markers. Here too, f_G increases with temperature [Fig. 4(d)]. In addition, we observe that the number of vortices connected to the blue network (N_B) initially increases more rapidly than those connected to the red network (N_R), giving rise to a peak in the ratio (N_B/N_R) [inset Fig. 4(d)]. This can be understood as follows. The red network arises from a change of position of a $G_N(V, \mathbf{r})$ minimum which happens whenever the vortex gets trapped in a pinning center between two local minima in $G_N(V, \mathbf{r})$. As the temperature is increased these trapping events become rarer and the vortex movement predominantly involves hops between two $G_N(V, \mathbf{r})$ minima that leave their

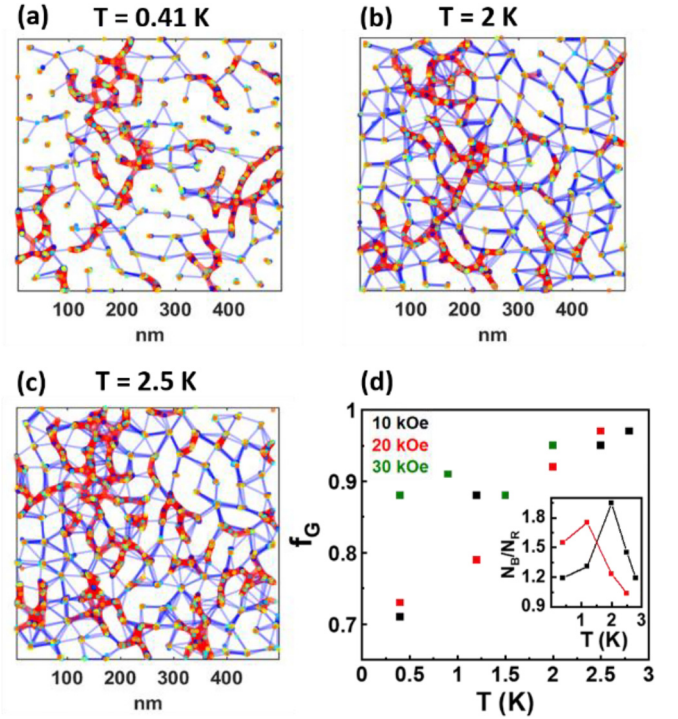


FIG. 4. (a)–(c) Positions of $G_N(V, \mathbf{r})$ minima from ten consecutive images taken at 10 kOe at different temperatures along with global motion paths of vortices; the color scheme is the same as Fig. 2(d). (d) f_G vs T for 10, 20, and 30 kOe. Inset: (N_B/N_R) variation with temperature for 10 and 20 kOe, respectively.

positions unchanged. (The opposite happens at very low fields, i.e., 1 kOe, and low temperatures where the minima are far apart and a complete hop from one minimum to another becomes extremely rare [36].) Above the peak temperature the red network also increases and (N_B/N_R) approaches unity. We believe that this decrease marks the gradual crossover towards a homogeneous unpinned liquid as theoretically predicted [21,44]. Above 2.8 K we cannot resolve minima in $G_N(V, \mathbf{r})$ anymore. A similar temperature evolution is also observed [36] at 20 kOe.

Based on the insight obtained from STS we can try to qualitatively understand other transport peculiarities such as low onset of nonlinear creep [20,45] and the formation of vortex slush [23–25] earlier reported in superconducting films. In Fig. 5, we plot (in log-log scale) the differential resistance $R = \frac{dV}{dI}$ as a function of current at 20 kOe, obtained from the I - V characteristics of our thin film. We observe that the current, I_{nl} , at which nonlinear creep sets in gradually shrinks to smaller values as the temperature is decreased. Estimating I_{nl} from the value at which [20] $\frac{\partial \ln(V)}{\partial \ln(I)} = 1.2$, we observe that I_{nl} follows a power law $I_{nl} \propto T^{2.91}$ (see inset of Fig. 5) so that it becomes vanishingly small [46] in the limit $T \rightarrow 0$. The vortex slush is characterized by the S shape of the R - I curve, where R appears to plateau at a temperature independent value much lower than the flux-flow resistance R_{ff} . In Fig. 5, we observe the vortex slush behavior below 1.4 K. Both these features can be understood from the percolative transport network that we observe in our experiments. Just like temperature or magnetic field, with increase in current the percolative network will

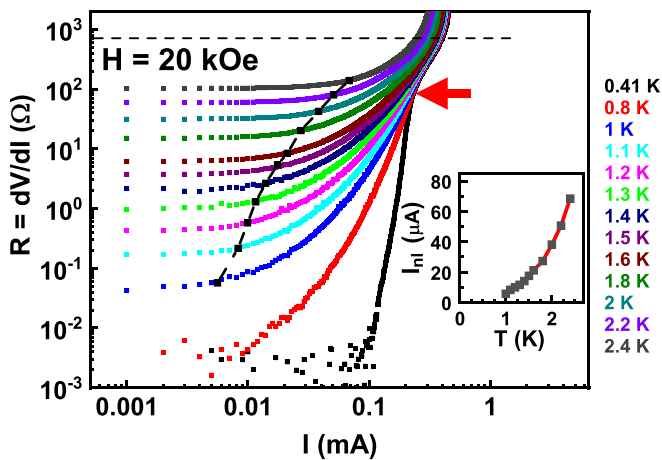


FIG. 5. R vs I plotted in log-log scale for various temperature at 20 kOe. The black squares show the onset of nonlinear flux creep on the R - I curves; the connecting dashed line is a guide to the eye. The red arrow points to the vortex slush behavior. The horizontal dashed line shown the value of R_{ff} at 0.41 K; Inset: Variation of I_{nl} with temperature following a power law $I_{nl} \propto T^{2.91}$ (solid line).

get denser such that the number of vortices participating in dissipation will increase continuously with applied current. This would give a faster than linear increase the voltage at low currents. The vortex slush plateau is expected when the network connects all vortices. At this drive all vortices are mobile but the average mobility will be smaller than that expected

for Bardeen-Stephen flux flow due to the underlying pinning potential. As the current is further increased the resistance gradually crosses over to the flux flow regime.

In summary, we show the existence of an inhomogeneous VL in an a -ReZr film formed under the combined influence of intervortex interactions and defect pinning. Even though our work focused on 5-nm-thick a -ReZr film, a similar pinned vortex liquid is also seen in a 2-nm-thick a -MoGe thin film [36]. We conjecture that this is a general feature in ultrathin superconducting films, where the enhanced role of fluctuations prevents the formation of a vortex glass as in the case of bulk samples. If the pinned VL indeed survives down to $T = 0$, the pertinent question would be whether below a certain temperature it transforms into a quantum liquid and gives rise to the much-debated Bose metal [47–51,15]. Future STS studies in the presence of a current drive will provide further insight on the transport-structure correlation of the pinned VL state.

We thank I. Maccari and I. Roy for valuable suggestions. The work was supported by the Department of Atomic Energy, Government of India. R.D., S.B., and V.B. synthesized the sample and performed basic characterization. R.D. performed STS measurements and analyzed the data. S.S. and R.T. performed magnetotransport measurements and analyzed the data. C.D. provided theoretical support. P.R. conceived the problem, supervised the experiments, and wrote the manuscript. All authors read and commented on the manuscript.

- [1] P. Berghuis, A. L. F. van der Slot, and P. H. Kes, Dislocation-mediated vortex-lattice melting in thin films of a -Nb₃Ge, *Phys. Rev. Lett.* **65**, 2583 (1990).
- [2] I. Guillamón, H. Suderow, A. Fernández-Pacheco, J. Sesé, R. Córdoba, J. M. De Teresa, M. R. Ibarra, and S. Vieira, Direct observation of melting in a two-dimensional superconducting vortex lattice, *Nat. Phys.* **5**, 651 (2009).
- [3] I. Guillamón, R. Córdoba, J. Sesé, J. M. De Teresa, M. R. Ibarra, S. Vieira, and H. Suderow, Enhancement of long-range correlations in a 2D vortex lattice by an incommensurate 1D disorder potential, *Nat. Phys.* **10**, 851 (2014).
- [4] I. Roy, S. Dutta, A. N. Roy Choudhury, S. Basistha, I. Maccari, S. Mandal, J. Jesudasan, V. Bagwe, C. Castellani, L. Benfatto, and P. Raychaudhuri, Melting of the vortex lattice through intermediate hexatic fluid in an a -MoGe thin film, *Phys. Rev. Lett.* **122**, 047001 (2019).
- [5] H. Pastoriza, M. F. Goffman, A. Arribere, and F. de la Cruz, First order phase transition at the irreversibility line of Bi₂Sr₂CaCu₂O₈, *Phys. Rev. Lett.* **72**, 2951 (1994).
- [6] E. Zeldov, D. Majer, M. Konczykowski, V. B. Geshkenbein, V. M. Vinokur, and H. Shtrikman, Thermodynamic observation of first-order vortex-lattice melting transition in Bi₂Sr₂CaCu₂O₈, *Nature (London)* **375**, 373 (1995).
- [7] S. S. Banerjee, S. Goldberg, A. Soibel, Y. Myasoedov, M. Rappaport, E. Zeldov, F. de la Cruz, C. J. van der Beek, M. Konczykowski, T. Tamegai, and V. M. Vinokur, Vortex nanoliquid in high-temperature superconductors, *Phys. Rev. Lett.* **93**, 097002 (2004).
- [8] L. Li, J. G. Checkelsky, S. Komiya, Y. Ando, and N. P. Ong, Low-temperature vortex liquid in La_{2-x}Sr_xCuO₄, *Nat. Phys.* **3**, 311 (2007).
- [9] E. M. Forgan, S. J. Levett, P. G. Kealey, R. Cubitt, C. D. Dewhurst, and D. Fort, Intrinsic behavior of flux lines in pure niobium near the upper critical field, *Phys. Rev. Lett.* **88**, 167003 (2002).
- [10] C. J. Howell, R. J. Lycett, M. Laver, C. D. Dewhurst, R. Cubitt, and E. M. Forgan, Absence of vortex lattice melting in a high-purity Nb superconductor, *Phys. Rev. B* **82**, 144508 (2010).
- [11] S. S. Banerjee, S. Ramakrishnan, A. K. Grover, G. Ravikumar, P. K. Mishra, V. C. Sahni, C. V. Tomy, G. Balakrishnan, D. Mck. Paul, P. L. Gammel, D. J. Bishop, E. Bucher, M. J. Higgins, and S. Bhattacharya, Peak effect, plateau effect, and fishtail anomaly: The reentrant amorphization of vortex matter in 2H-NbSe₂, *Phys. Rev. B* **62**, 11838 (2000).
- [12] M. Zehetmayer, How the vortex lattice of a superconductor becomes disordered: A study by scanning tunneling spectroscopy, *Sci. Rep.* **5**, 9244 (2015).
- [13] S. C. Ganguli, H. Singh, G. Saraswat, R. Ganguly, V. Bagwe, P. Shirage, A. Thamizhavel, and P. Raychaudhuri, Disordering of the vortex lattice through successive destruction of positional and orientational order in a weakly pinned Co_{0.0075}NbSe₂ single crystal, *Sci. Rep.* **5**, 10613 (2015).
- [14] S. Dutta, I. Roy, J. Jesudasan, S. Sachdev, and P. Raychaudhuri, Evidence of zero-point fluctuation of vortices in a very

- weakly pinned a-MoGe thin film, *Phys. Rev. B* **103**, 214512 (2021).
- [15] S. Dutta, J. Jesudasan, and P. Raychaudhuri, Magnetic field induced transition from a vortex liquid to Bose metal in ultrathin a-MoGe thin film, *Phys. Rev. B* **105**, L140503 (2022).
- [16] A. I. Larkin and Y. N. Ovchinnikov, Pinning in type II superconductors, *J. Low Temp. Phys.* **34**, 409 (1979).
- [17] M. V. Feigel'man, V. B. Geshkenbein, A. I. Larkin, and V. M. Vinokur, Theory of collective flux creep, *Phys. Rev. Lett.* **63**, 2303 (1989).
- [18] D. S. Fisher, M. P. A. Fisher, and D. A. Huse, Thermal fluctuations, quenched disorder, phase transitions, and transport in type-II superconductors, *Phys. Rev. B* **43**, 130 (1991).
- [19] V. M. Vinokur, P. H. Kes, and A. E. Koshelev, Flux pinning and creep in very anisotropic high temperature superconductors, *Phys. C (Amsterdam, Neth.)* **168**, 29 (1990).
- [20] C. Dekker, P. J. M. Wöltgens, R. H. Koch, B. W. Hussey, and A. Gupta, Absence of a finite-temperature vortex-glass phase transition in two-dimensional $\text{YBa}_2\text{Cu}_3\text{O}_{7-\delta}$ films, *Phys. Rev. Lett.* **69**, 2717 (1992).
- [21] V. M. Vinokur, M. V. Feigel'man, V. B. Geshkenbein, and A. I. Larkin, Resistivity of High- T_c Superconductors in a Vortex-Liquid State, *Phys. Rev. Lett.* **65**, 259 (1990).
- [22] C. Dasgupta and O. T. Valls, Phase diagram of the vortex system in layered superconductors with strong columnar pinning, *Phys. Rev. B* **72**, 094501 (2005).
- [23] T. K. Worthington, M. P. A. Fisher, D. A. Huse, John Toner, A. D. Marwick, T. Zabel, C. A. Feild, and F. Holtzberg, Observation of separate vortex-melting and vortex-glass transitions in defect-enhanced $\text{YBa}_2\text{Cu}_3\text{O}_{7-\delta}$ single crystals, *Phys. Rev. B* **46**, 11854 (1992).
- [24] W. Zhao, C-Z. Chang, X. Xi, K. F. Mak, and J. S. Moodera, Vortex phase transitions in monolayer FeSe film on SrTiO_3 , *2D Mater.* **3**, 024006 (2016).
- [25] M. Andersson, P. Fivat, L. Fàbrega, H. Obara, M. Decroux, J.-M. Triscone, and O. Fischer, Vortex solid-to-liquid transition in $\text{DyBa}_2\text{Cu}_3\text{O}_{7-\delta}/(\text{Y}_{0.45}\text{Pr}_{0.55})\text{Ba}_2\text{Cu}_3\text{O}_{7-\delta}$ multilayers, *Phys. Rev. B* **54**, 675 (1996).
- [26] F. Wang, D. Zhou, and Y. Han, Melting of colloidal crystals, *Adv. Funct. Mater.* **26**, 8903 (2016).
- [27] P. Huang, T. Schönenberger, M. Cantoni, L. Heinen, A. Magrez, A. Rosch, F. Carbone, and H. M. Rønnow, Melting of a skyrmion lattice to a skyrmion liquid via a hexatic phase, *Nat. Nanotechnol.* **15**, 761 (2020).
- [28] S. Veatch, O. Soubias, S. Keller, and K. Gawrisch, Critical fluctuations in domain-forming lipid mixtures, *Proc. Natl Acad. Sci. USA* **45**, 17650 (2007).
- [29] H. Suderow, I. Guillamón, J. G. Rodrigo, and S. Vieira, Imaging superconducting vortex cores and lattices with a scanning tunneling microscope, *Supercond. Sci. Technol.* **27**, 063001 (2014).
- [30] A. Kamlapure, G. Saraswat, S. C. Ganguli, V. Bagwe, P. Raychaudhuri, and S. P. Pai, A 350 mK, 9 T scanning tunneling microscope for the study of superconducting thin films on insulating substrates and single crystals, *Rev. Sci. Instrum.* **84**, 123905 (2013).
- [31] A. M. Troyanovskii, J. Aarts, and P. H. Kes, Collective and plastic vortex motion in superconductors at high flux densities, *Nature (London)* **399**, 665 (1999).
- [32] E. Herrera, J. Benito-Llorens, U. S. Kaluarachchi, S. L. Bud'ko, P. C. Canfield, I. Guillamón, and H. Suderow, Vortex creep at very low temperatures in single crystals of the extreme type-II superconductor $\text{Rh}_9\text{In}_5\text{S}_4$, *Phys. Rev. B* **95**, 134505 (2017).
- [33] R. Willa, J. Augusto Galvis, J. Benito-Llorens, E. Herrera, I. Guillamon, and H. Suderow, Thermal creep induced by cooling a superconducting vortex lattice, *Phys. Rev. Res.* **2**, 013125 (2020).
- [34] G. I. Menon, C. Dasgupta, H. R. Krishnamurthy, T. V. Ramakrishnan, and S. Sengupta, Density-functional theory of flux-lattice melting in high- T_c superconductors, *Phys. Rev. B* **54**, 16192 (1996).
- [35] S. Dutta, V. Bagwe, G. Chaurasiya, A. Thamizhavel, R. Bapat, P. Raychaudhuri, and S. Bose, Superconductivity in amorphous Re_xZr ($x \approx 6$) thin films, *J. Alloys Compd.* **877**, 160258 (2021).
- [36] See Supplemental Material at <http://link.aps.org/supplemental/10.1103/PhysRevB.108.L180503> for further details on sample characterization, data analysis, temperature dependence of global motion paths, vortex liquid behavior at 1 kOe, hierarchy of pinning strength, global motion path in vortex solid and liquid in a 20-nm-thick a- Re_xZr film, and the pinned vortex liquid in ultrathin a-MoGe film.
- [37] M. Buchacek, Z. L. Xiao, S. Dutta, E. Y. Andrei, P. Raychaudhuri, V. B. Geshkenbein, and G. Blatter, Experimental test of strong pinning and creep in current-voltage characteristics of type-II superconductors, *Phys. Rev. B* **100**, 224502 (2019).
- [38] D. Ephron, A. Yazdani, A. Kapitulnik, and M. R. Beasley, Observation of quantum dissipation in the vortex state of a highly disordered superconducting thin film, *Phys. Rev. Lett.* **76**, 1529 (1996).
- [39] O. Brunner, L. Antognazza, J.-M. Triscone, L. Mieville, and O. Fischer, Thermally activated flux motion in artificially grown $\text{YBa}_2\text{Cu}_3\text{O}_{7-\delta}/\text{PrBa}_2\text{Cu}_3\text{O}_7$ Superlattices, *Phys. Rev. Lett.* **67**, 1354 (1991).
- [40] A. W. Tsen, B. Hunt, Y. D. Kim, Z. J. Yuan, S. Jia, R. J. Cava, J. Hone, P. Kim, C. R. Dean, and A. N. Pasupathy, Nature of the quantum metal in a two-dimensional crystalline superconductor, *Nat. Phys.* **12**, 208 (2016).
- [41] H. K. Kundu, K. R. Amin, J. Jesudasan, P. Raychaudhuri, S. Mukerjee, and A. Bid, Effect of dimensionality on the vortex dynamics in a type-II superconductor, *Phys. Rev. B* **100**, 174501 (2019).
- [42] M. V. Feigelman, V. B. Geshkenbein, and A. I. Larkin, Pinning and creep in layered superconductors, *Phys. C (Amsterdam, Neth.)* **167**, 177 (1990).
- [43] B. van der Meer, W. Qi, J. Sprakel, L. Filiona, and M. Dijkstra, Dynamical heterogeneities and defects in two-dimensional soft colloidal crystals, *Soft Matter* **11**, 9385 (2015).
- [44] C. Dasgupta and O. T. Valls, Phase diagram of vortex matter in layered high-temperature superconductors with random point pinning, *Phys. Rev. B* **74**, 184513 (2006).
- [45] A. Benyamini, E. J. Telford, D. M. Kennes, D. Wang, A. Williams, K. Watanabe, T. Taniguchi, D. Shahar, J. Hone, C. R. Dean, A. J. Millis, and A. N. Pasupathy, Fragility of the dissipationless state in clean two-dimensional superconductors, *Nat. Phys.* **15**, 947 (2019).
- [46] In Ref. [20], the temperature exponent of 3 for I_{nl} has been attributed to a vortex glass transition at zero temperature.

- [47] P. Phillips and D. Dalidovich, The elusive Bose metal, *Science* **302**, 243 (2003).
- [48] J. Wu and P. Phillips, Vortex glass is a metal: Unified theory of the magnetic-field and disorder-tuned Bose metals, *Phys. Rev. B* **73**, 214507 (2006).
- [49] B. Spivak, P. Oredo, and S. A. Kivelson, Theory of quantum metal to superconductor transitions in highly conducting systems, *Phys. Rev. B* **77**, 214523 (2008).
- [50] C. Yang, Y. Liu, Y. Wang, L. Feng, Q. He, J. Sun, Y. Tang, C. Wu, J. Xiong, W. Zhang, X. Lin, H. Yao, H. Liu, G. Fernandez, J. Xu, J. M. Valles, Jr., J. Wang, and Y. Li, Intermediate bosonic metallic state in the superconductor-insulator transition, *Science* **366**, 1505 (2019).
- [51] T. Ren and A. M. Tsvelik, How magnetic field can transform a superconductor into a Bose metal, *New J. Phys.* **22**, 103021 (2020).